TRANSACTIONS OF THE INSTITUTE OF FLUID-FLOW MACHINERY

No. 126, 2014, 55–64

LÁSZLÓ KALMÁR[a] *, GÁBOR JANIGA[b], BÉLA FODOR[a] and LÁSZLÓ SOLTÉSZ[c]

# Characterization of different one-stage blower designs using three-dimensional unsteady numerical flow simulation

[a] *University of Miskolc, The Department of Fluid and Heat Engineering, Egytemvaros, 3515 Hungary.*

[b] *University of Magdeburg „Otto-von-Guericke", Lab. of Fluid Dynamics and Technical Flows, Universitatsplatz 2, 39106 Magdeburg, Germany.*

[c] *Electrolux Lehel Ltd., Small Appliance Factory, Erzebet Kiralyne 87, 1142 Budapest Hungary.*

**Abstract**

This paper deals with the computational fluid dynamics investigation of the flow in a one-stage radial flow blower-aggregate. The main aim of this numerical study is to compute the relevant operating characteristics of the blower and to determine detailed information about the flow characteristics inside it. The distributions of these flow characteristics in the blower determined by the commercial code are available to judge whether the elements of the blower are working properly, or not. The calculated characteristics of operating parameters are compared with measured data given by experimental tests of the blower-aggregate for their validation.

**Keywords:** Blower; Numerical simulation; Unsteady flow

## 1 Introduction

The investigated blower aggregate, noted by B$A0$ can be seen in Fig. 1 and the same aggregate is shown in Fig. 2 in a disassembled state to introduce the main parts of the blower.

The first step of our numerical investigation was to create the complete computational domain of the blower-aggregate. It has been produced in the commercial

*Corresponding author. E-mail address: aramka@uni-miskolc.hu

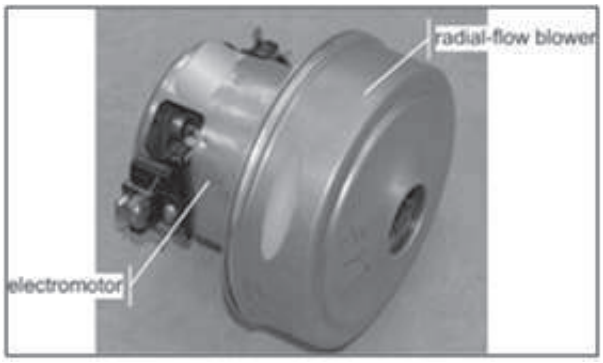


Figure 1. Photo of the investigated blower aggregate B*A0*.

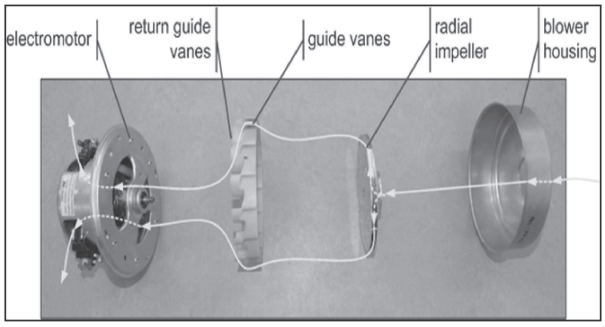


Figure 2. Main components of the blower aggregate B*A0*.

preprocessing tool. The entire three-dimensional computational domain of the blower aggregate is illustrated in Fig. 3 in two different views. By comparing the photos of the blower (Figs. 1–2) and the 3D drawing of the aggregate model (Fig. 3) it is easy to realise that the inlet and outlet parts of the model are slightly modified.

Figure 3. The three-dimensional computational domain of the blower aggregate B*A0*.

At the inlet cross section of the blower – to produce relatively homogeneous velocity distribution along the inlet cross section during the numerical simulation

– a cylindrical short pipe section with circular cross section was connected. At the outlet section of the blower two short cylindrical pipe sections were connected with the similar shape of the cross section which can be seen in the wall between the blower and electromotor (see Fig. 2).

In Fig. 3 the inlet and outlet sections and the house of the blower can be seen. During the numerical simulation the total 3D computational domain (Fig. 3) also contains the rotating impeller (Fig. 4) and the stationary guide vanes and the stationary return guide vanes (see Fig. 5) of the blower, which can be found inside the blower house. The air flows into the blower throughout the inlet section and arrives to the impeller, then flows across it which increases the total energy of the air. After first the air flows in the guide vanes at impeller side then flows in the guide vanes on the back side. Finally the air flows through the pressured side of the blower and leaves the blower throughout the outlet sections.

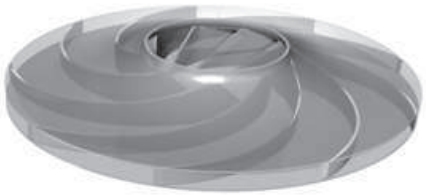

Figure 4. The three-dimensional computational domain of the impeller of the blower aggregate B*A0*.

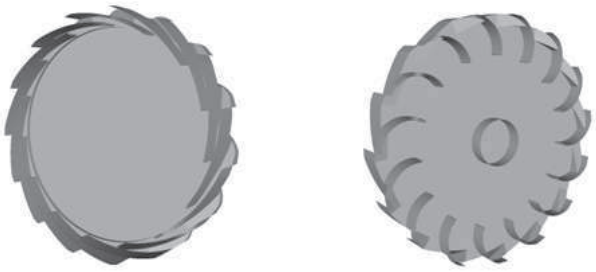

Figure 5. The three-dimensional computational domain of the guide vanes of the blower aggregate B*A0*.

The main aim of this numerical investigation is to determine the relevant operating characteristics of the blower by compputational fluid dynamics (CFD) numerical methods.

## 2 Computational configuration

To carry out the numerical simulation of flow in blower, the total computational domain has to be divided into subdomains, as shown in Fig. 6. Two types of important subdomains have to be detached because of their operations: the rotational subdomain (named ROTOR) is the subdomain of the blower impeller and the stationary subdomains (named STATOR) which are bounded by the walls of the blower, the guide vanes and return guide vanes.

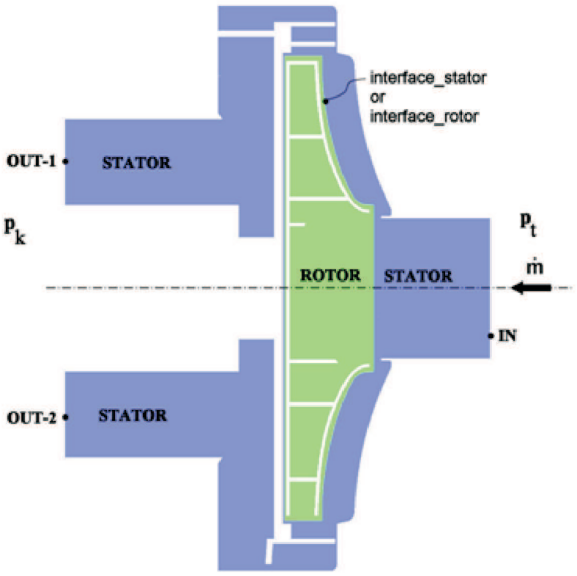


Figure 6. Partitioning of the computational domain.

## 3 Computational methods

The 'finite volume' method is applied to determine the solution of the flow problems. That is why before starting to run the code all the subdomains have to be divided into finite volumes. In other words, we have to mesh the total computational domain. When carrying out this procedure we have to pay extra attention to the geometrical characteristics of each finite element. The mesh generation was carried out with the commercial code. To get information about the quality of mesh elements it is the most convenient way to display the actual values of the cells skewness. In our case 5.03 million finite volumes were developed and the measured maximum value was equal to 0.8082, which means that the quality of

the meshing is acceptable to perform the CFD computation. Some details of the computational mesh of the impeller are illustrated in Fig. 7.

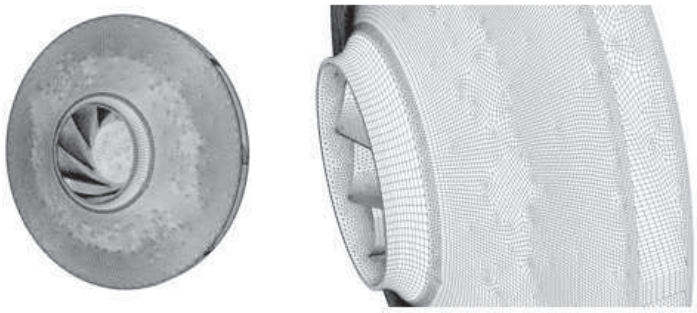

Figure 7. The computational mesh of the impeller surface of the blower aggregate B*A0*.

## 4 Computational results

For all the cells of the total computational domain the 'density based implicit Gauss-Seidel' numerical solver was used during the numerical solution process assuming unsteady flow. Because during the operations of blower relatively high velocities and pressures increase take place, it was also supposed that the fluid was compressible and viscous. In this way the standard $k$-$\omega$ SST (sher stress transport) turbulent models and perfect-gas law were applied in our simulations. The results obtained CFD simulation are illustrated next. Figures 9–10 show the local distributions of the velocity and absolute or dynamic pressure fields, while all the diagrams give information about the variations of average absolute or dynamic pressure, density and the mass-flow (concerning to the denoted 16 different sections of the flow in Fig. 8) in direction of the main flow inside the aggregate.

In Fig. 9A the distributions of relative (inside the impeller) and absolute (inside the guide vanes) velocity fields are shown along plane A. Figure 9B shows the distribution of absolute velocity (inside the return guide vanes and the pressured side of the blower) along plane B. Figure 10A shows the distribution of absolute pressure field inside the impeller and guide vanes along plane A. In Fig. 10B the distributions of absolute pressure in return guide vanes and the pressured side of the blower are shown along plane B. Figures 9 and 10 give insight into the local structures of the flow using streamlines along the two planes denoted by A and B. By using our developed numerical model three different operating points of the blower aggregate B*A0* were numerically investigated by CFD. One of the initial parameters of our calculation was the mass-flow rate at inlet, and the actual pres-

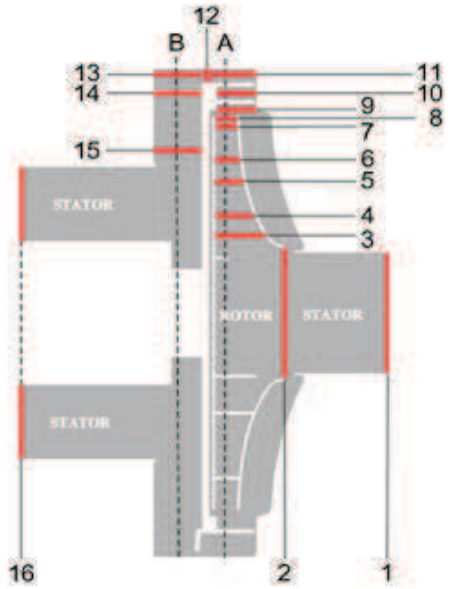


Figure 8. Positions of sections 1-16 of the flow and two planes of A and B.

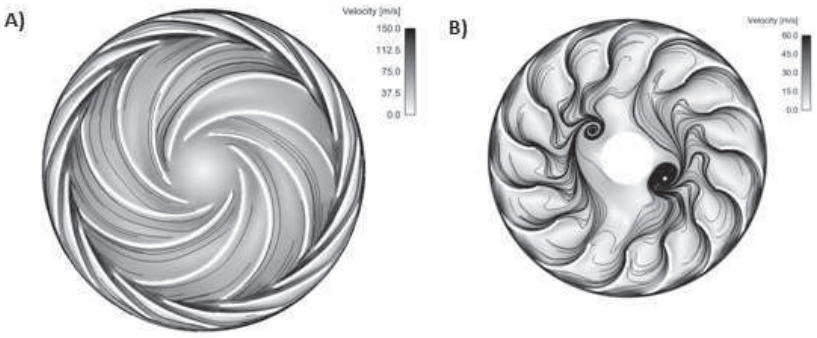


Figure 9. Velocity field along plane A and B of the blower aggregate B*A0*.

sure difference between the outlet and inlet sections of the blower was calculated in this way. For validation of our calculation we compared the characteristics of three calculated working points determined separately by actual values of the mass flow rates $\dot{m}_I = 0.046$ kg/s, $\dot{m}_{II} = 0.033$ kg/s and $\dot{m}_{III} = 0.022$ kg/s with the measured characteristic curve of the blower aggregate B*A0* given by laboratory tests [1], which are shown in Fig. 11. A very good agreement can be observed in this figure.

The CFD investigations introduced above are also carried out for additional

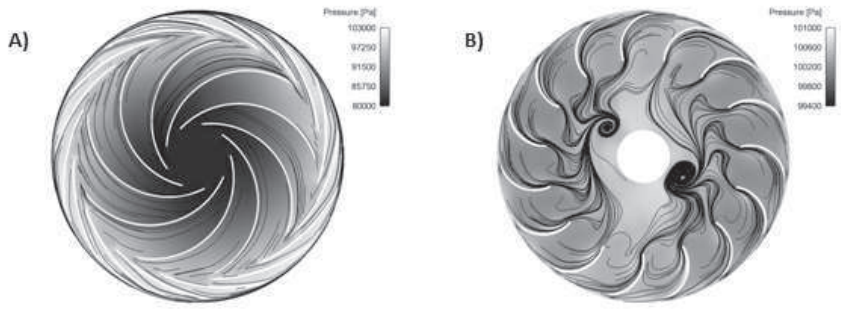


Figure 10. Absolute pressure field along plane A and B of the blower aggregate B*A0*.

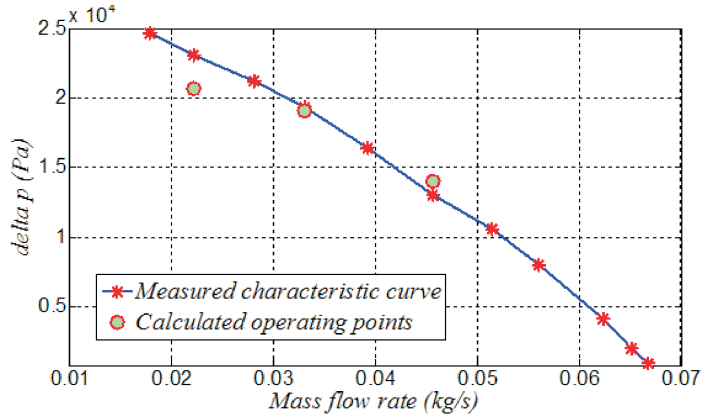


Figure 11. Calculated working points and measured characteristic curve of the blower aggregate B*A0*.

two different blower aggregates noted by B*A1* and B*A2*. The blower aggregates B*A1* and B*A2* are very similar to blower aggregate B*A0* except the following differences:

- the blower aggregate B*A1* has newly designed stationary guide vanes and the stationary return guide vanes with new geometries,
- the blower aggregate B*A2* has newly designed radial flow impeller, re-designed stationary guide vanes and the stationary return guide vanes with new geometries.

Figures 12–15 show the variations of averaged flow parameters which are determined by surface integration of physical fields concerning the blower aggregates B*A0*, B*A1* and B*A2*. All of them are determined for operation state at mass flow rate $\dot{m}_{II} = 0.033$ kg/s of the blower aggregates.

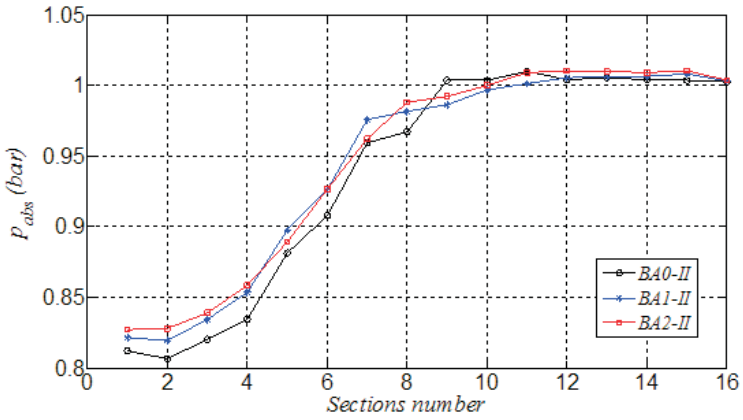


Figure 12. Variation of absolute pressure.

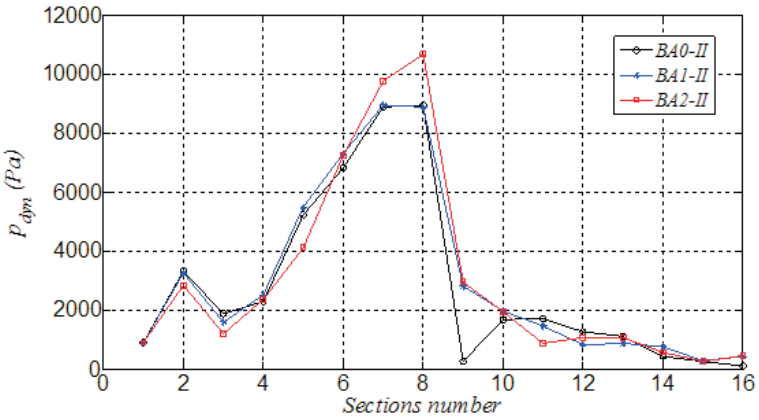


Figure 13. Variation of dynamic pressure.

Knowing the variations of these averaged parameters is very important, if we want to get useful information about the operational characteristics of the blower. The sixteen different cross-sections can be seen (see Fig. 8). The average values of absolute, dynamic pressures and density were determined by surface integration for the denoted 16 sections and the variations of these flow characteristics are shown in Figs. 12-14. The values of mass flow rate concerning these cross sections are also calculated and shown in Fig. 15.

In this way in Figs. 12 and 13 between sections 2 and 8 (inside the impeller) the variations of absolute and dynamic pressure show the energy increase through the impeller. Between sections 8 and 10 the increase in cross sectional area causes

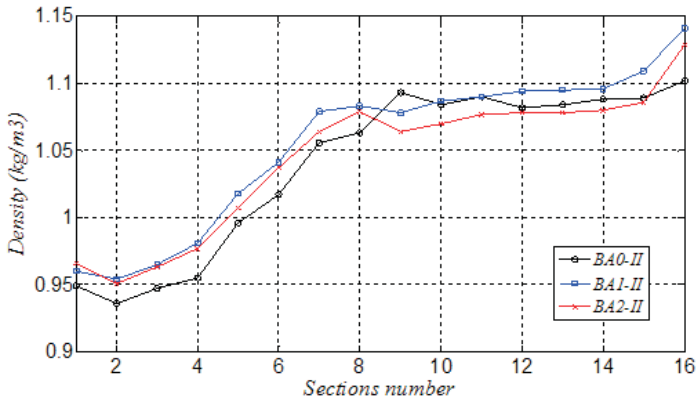


Figure 14. Variation of air density.

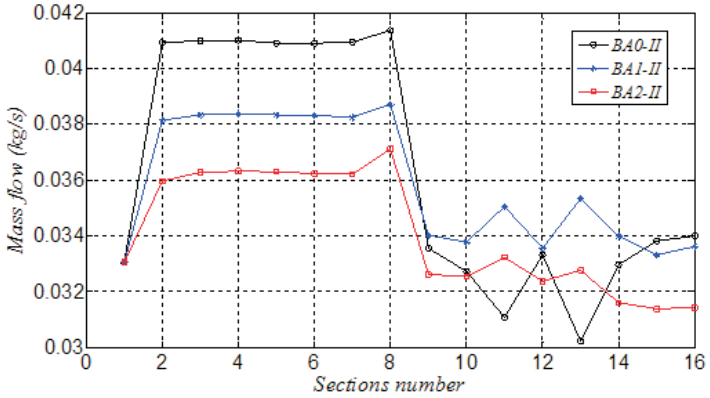


Figure 15. Variation of mass flow.

a sudden drop in the dynamic pressure and a small increase in the absolute pressure. In Fig. 15 between sections 2 and 8 the relatively large increase caused by leakage.

## 5 Summary

This study has demonstrated that numerical flow simulations are able to provide detailed information about the local flow structures supporting the design process. These structures are introduced, e.g., in Fig. 9A illustrating the stagnation surfaces or in Fig. 10B showing the vortical structures in return guide vanes. All these effects diminish the efficiency of the machine; therefore, they should be eliminated as possible.

**Acknowledgements** The work was carried out as part of the TÁMOP-4.2.1.B-10/2/KONV-2010-0001 project in the framework of the New Hungarian Development Plan. The realization of this project is supported by the European Union, co-financed by the European Social Fund.

Received 15 October 2014

## References

[1] Lakatos, K., Szaszák, N., Mátrai Zs., Soltész L., Szabó Sz.: *Development of Guide Vanes and Return Guide Vanes of a Mini Blower.* Proc. MicroCAD Int. Computer Sci. Conf., Miskolc 2011, 65–72.